metals

MDPI

Article

An Equivalent Calculation Method for Press-Braking Bending Analysis of Integral Panels

Min Zhang, Xitian Tian *, Wupeng Li and Xiaolin Shi

School of Mechanical Engineering, Northwestern Polytechnical University, Xi'an 710072, China; zhangmin0907@mail.nwpu.edu.cn (M.Z.); 1126470795@mail.nwpu.edu.cn (W.L.); sxl86@mail.nwpu.edu.cn (X.S.)
* Correspondence: tianxt@nwpu.edu.cn; Tel.: +86-29-8849-5445

Received: 17 April 2018; Accepted: 15 May 2018; Published: 18 May 2018

Abstract: Press-braking bending is widely applied in the manufacture of aircraft integral panels because of the advantages of strong adaptability to different contours, simplicity of bending tools, short manufacturing time and low process cost. However, a simulation of bending process requires long-time calculation and consumes extensive computational resources. Considering the factors that the original model (ORM) of an integral panel is large and the press-braking bending is used only for the local area of integral panels with heavy thickness in practice, an equivalent calculation method for press-braking bending analysis of integral panels is proposed. The local bending area of an integral panel is simplified to a model of plate in this method. An exponential strengthening model is used to derive the equations of stress, strain and forming radius of the ORM and its simplified model (SPM). Meanwhile, the equivalent parameters of the SPM are determined and deduced based on three principles: that the material begin to be yielded simultaneously, the ultimate stress of the ORM is the same as that of the SPM at the same punch displacement, and the forming radii of neutral surfaces of the ORM and the SPM are identical after springback. The distribution of the stress and strain determined by finite element (FE) simulations are compared, and the FE simulations indicate that the contour curve of the SPM is in fairly good agreement with the profile of the ORM under the same bending process parameters, and the maximum difference is 13.17%. The computational efficiency is increased by more than 48%. Therefore, the proposed approach is quite suitable for industrial applications to improve the bending quality and efficiency of integral panels.

Keywords: equivalent model; press-braking bending; equivalent parameters; finite element (FE) method; integral panels

1. Introduction

Aircraft integral panels have been widely used in aerospace vehicles due to their advantages of lightweight design, high strength, and high structural efficiency [1–3]. Because of the large thickness and high strength of integral panels, press-braking bending has become a common method for the manufacture of integral panels. The basic advantages are economical set-up as well as the enormous range of part size and complex shape that can be fabricated [4], short manufacturing time and low process cost [5–7]. Now, there are many aircrafts made by this forming method, such as Ukraine An series large transport aircrafts, Russia Su-27, Su-303, fourth-generation fighters and the aircrafts with high rib net panels. However, for the operators, achieving the target shape of a formed product is challenging [8]. Otherwise, they need to spend a lot of time afterwards to modify process parameters. It is easy to cause the following defects: low precision of the contours, difficulty controlling the forming process, and sometimes fractures may occur and lead to the integral panels being completely scrapped [9]. In addition, the materials of integral panels are expensive and the bending process is the last step in the manufacturing process. Therefore, the aforementioned defects can cause great economic

losses [10] and project delay, and seriously affect the quality and efficiency of aircraft assembly. In order to improve the forming accuracy of the final shape and lower the time cost, FE simulation has been considered an effective tool for simulating the forming process, optimizing the forming parameters and predicting the forming results in order to replace the time consuming and costly "trial and error" method in actual fabrication [11–13]. Hence, the establishment of a reliable FE simulation model is the key to studying the complex forming process of integral panels.

A considerable amount of research on numerical analysis of sheet metal forming process has been performed [14]. An FE model of U-shape channel was built by Ghaei [15] to simulate the forming stage and springback stage using Abaqus/Explicit and Abaqus/Standard, respectively. A 3D dynamic FE model of an asymmetrical roll bending process is developed by Tran [16] to investigate the parameters that affect the accuracy of the final shape, the bending forces and the residual strains left in the formed plate. A three-dimensional FE model of the rotary-draw bending process of a thin-walled rectangular tube is built under the Abaqus/explicit environment by Zhao [17]. Fu [18,19] established a FE model to simulate the multiple-step incremental air-bending forming and springback processes. Henrard et al. [20] studied the accuracy of FE simulations in predicting the tool force occurring during the single point incremental forming (SPIF) process. Bui et al. [21] employed a 3D finite element analysis to simulate a cold roll-forming process and useful information like the stress/strain distribution and the final geometry after springback was obtained.

However, there are still several difficulties during the establishment of FE simulation models for the bending and forming of aircraft panels. Firstly, the dimensions of an aircraft integral panel are quite large, and the stiffeners are plentiful and complicated, which lead to tremendous meshing and calculating time. Secondly, this press-braking bending process consists of multiple times of bending and springback. It is difficult to optimize the bending process by repeating calculations through FE simulation with the ORM of an integral panel, and the complicated contact conditions may lead to convergence problems. Thirdly, the press-braking bending is used only for the local area of integral panels with heavy thickness in practice; the calculation time must be immensely extended if the ORM is adopted. It is necessary to look for an equivalent calculation method to simplify the area that is not directly involved in bending load applying, instead of the complex bending process of an ORM.

Researchers have studied and established some equivalent models for the stiffened plates adopting different methods. Yan [22] simplified the integral panel with reinforced structures as a plate with virtual material for bending analysis by elastic-plastic mechanics and springback analysis, and then an equivalent finite element simulation model of reinforced panels was established. Li [7] proposed a geometrical equivalent method, which simplified the skin components to stiffener with virtual material properties. Three equivalent methods of a honeycomb sandwich had been studied by Xia [23] and Zhang [24]. The equivalent mechanical parameters of honeycomb sandwich plates were obtained with mechanical analysis of elastic properties by Liang [25] and Chen [26]. Yang et al. [27] developed a 3D homogenization method to improve the accuracy of the equivalent models of the trapezoidal corrugated core.

Although the accuracy of the equivalent models established by the aforementioned literature is acceptable, the following limitations still exist: (1) The errors because of the integrally stiffened panel being directly equivalent to a rectangular thin plate are large due to the structure changes; (2) The stress and strain distribution of the forming process are not analyzed and evaluated in detail; (3) The main equivalent parameters are almost not analyzed, and the consistency of the contours between the ORM and the SPM should be guaranteed as far as possible under the same bending process parameters; (4) The equivalent methods of the sandwich panels are only applicable to the elastic deformation stage, while press-braking bending is a plastic deformation of the material subjected to bending moment [28]. Plastic properties should be considered during creation of the SPM for the forming process of the ORM.

In this work, an equivalent calculation approach for the press-braking bending of integral panels is developed without changing the structure of the area subjected to bending load. The bending forming process is presented firstly. Then an exponential strengthening model is used to derive the

equations of stress, strain and forming radius of the ORM and SPM based on elastoplastic theory. Finally, the equivalent parameters of the SPM are determined and deduced based on three principles that the material begin to be yielded simultaneously, the ultimate stress of the ORM is the same as that of the SPM at the same punch displacement, and the forming radii of neutral surfaces of the ORM and the SPM are identical after springback. To verify the reliability and precision of the equivalent calculation method, the distribution of the stress and strain determined by FE simulations are compared, and the contours at the end of the forming process are also compared between the FE models and the experimental results.

2. Press-Braking Bending Process

Because of the heavy thickness and grid structure, integral panels are rigid and cannot be fully formed solely through the shot peening forming method. Currently, the forming process of large transport aircrafts still uses the method of press-braking bending, and peening forming as an auxiliary process. In this work, both the forming process of integral panels and the press-braking bending process for local area are studied, which lay the foundation for the subsequent equivalent calculation.

In order to simplify the experiment and simulation approach against real integral panel in factory, an experimental sample is designed based on a real aircraft integral panel according to geometrical similarity, as shown in Figure 1. The experimental sample is 200-mm long, 60-mm wide, and 7.5-mm thick. The thickness of the ribs is 2 mm.

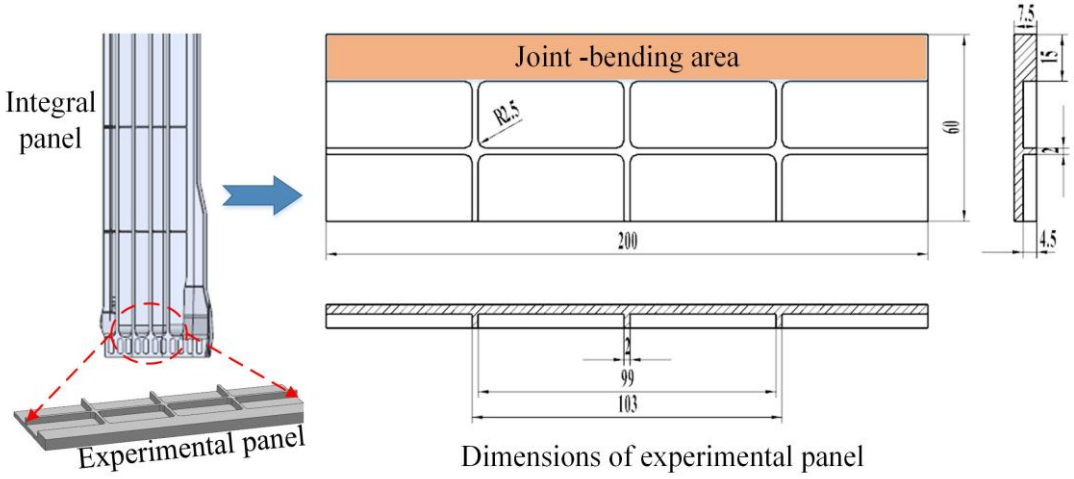

Figure 1. Experimental sample of an integral panel.

Figure 2 demonstrates the forming process of an integral panel. The process could be briefly described as follows: (1) A blank with the material of aluminum alloy 7050-T7451 is prepared; (2) A flat sheet is obtained by milling the upper and lower surfaces of the blank; (3) A panel with grid ribs is obtained by numerical control milling from the flat sheet; (4) The joint is adopted as the workpiece to be formed by the press-braking bending method; (5) Size detection is carried out to ensure the curvature of joint meets the requirements of manufacture; (6) Peening forming process as auxiliary process is adopted to form the grid and stiffeners; (7) and (8) are size detection and subsequent processing, respectively. The process of press-braking bending for joint (i.e., the step (4)) is the main content of this paper.

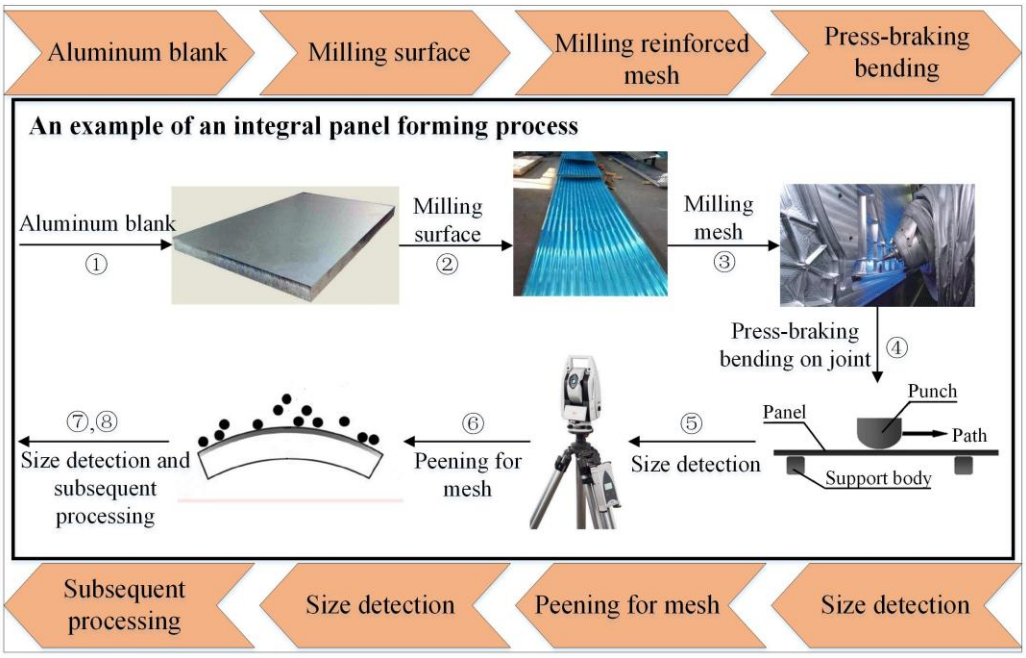

Figure 2. The forming process of an integral panel.

Figure 3 describes the loading sequence of press-braking bending, namely the step (4) shown in Figure 2. The span of the two support bodies is D. The diameter of the punch and the support bodies are d_1 and d_2, respectively. The load is applied step-by-step at the three pre-defined bending points (1), (2) and (3) with the sequence shown in Figure 3. The key principles of the bending process are: (a) the punch and support bodies are moved along the bending positions in an orderly manner; (b) the punch and support bodies are moved to the next position after the bending for one pressure point is finished; (c) the bending process is completed until the curvature meets the requirements of manufacture.

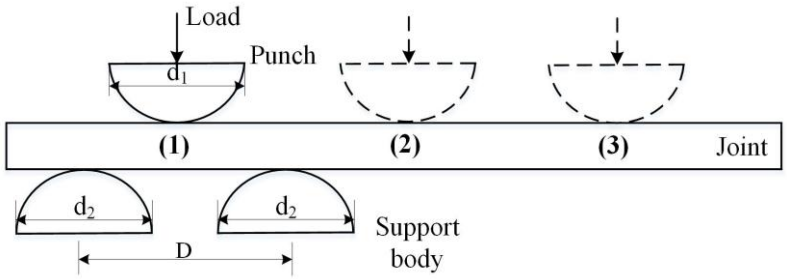

Figure 3. Loading sequence of press-braking bending.

3. Development of Equivalent Model

3.1. Equivalent Requirements

The basic equivalent requirements are to ensure that the material begins to be yielded simultaneously, the ultimate stress of the ORM is the same as that of the SPM at the same punch displacement, and the forming radii of the neutral surfaces of the ORM and the SPM are identical after complete springback. The key to establishing a SPM is to derive and calculate the equivalent parameters according to the mechanical properties of materials and the abovementioned constraints. The simplified process is presented in Figure 4. The bending area of the ORM is equivalent to a model of rectangular plate with the same thickness of ORM according to the conditions that the

geometrical shape and thickness have no changes. In Section 3.2, the bending forming of SPM is analyzed firstly. Then the bending forming of the ORM is analyzed by simplifying its cross section. Finally, the equivalent parameters of the SPM are obtained according to the equivalent requirements.

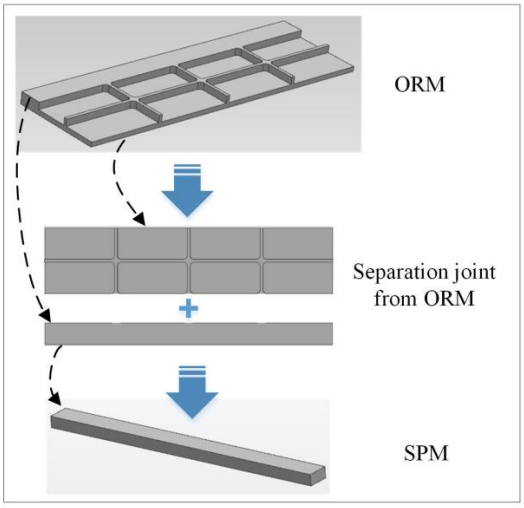

Figure 4. The simplified process.

3.2. Method

The equations of stress, strain and forming radius of the SPM and the ORM are analyzed respectively based on elastic-plastic mechanics. Finally, the equivalent parameters are obtained through equivalent requirements.

3.2.1. Bending Analysis of SPM

Assumptions for the bending analysis are summarized as follows:

- The material is isotropic and homogeneous.
- The plane section remains planar throughout deformation and springback.
- The change of thickness during bending is ignored.
- The neutral surface of bending is assumed to stay at the same position.
- The rolling direction of the material does not have a major impact on this forming process.

The section of the equivalent rectangular plate that wraps around the punch is taken as the investigation object in this study. The cross section of the SPM is shown in Figure 5.

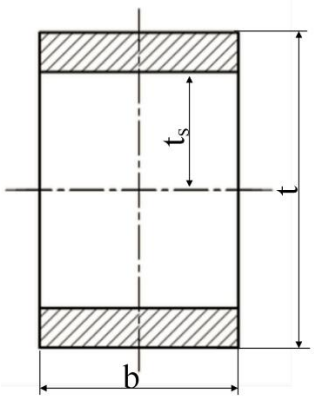

Figure 5. The cross section of a plate.

The relation between the stress and strain of the material satisfies the following exponential strengthening model [29]:

$$|\sigma| = \begin{cases} E|\varepsilon| & \text{if } |\sigma| \le \sigma_s \\ \sigma_s + K|\varepsilon_p|^n & \text{if } |\sigma| > \sigma_s \end{cases} \quad (1)$$

where E is the Young's modulus, σ_s is the yield stress, K is the hardening coefficient, n is the hardening exponent, and ε_p is the plastic strain which is approximately given by

$$|\varepsilon_p| = |\varepsilon| - |\varepsilon_e| \cong |\varepsilon| - \frac{\sigma_s}{E} \quad (2)$$

The elastic strain, ε_e, is approximated for simplicity by the strain at yield. The stress distribution along the thickness is given by

$$\sigma = \begin{cases} E\frac{y}{\rho} & |y| < t_s \\ \sigma_s + K\left(\frac{y}{\rho} - \frac{\sigma_s}{E}\right)^n & t_s \le |y| \le \frac{t}{2} \end{cases} \quad (3)$$

where

$$t_s = \frac{2\rho\sigma_s}{E} \quad (4)$$

Here, y is the distance between the material and neutral layer, ρ is the bending radius of the neutral layer, t is the thickness of the plate, t_s is half the thickness of elastic deformation.

When the stress of the outermost material reaches Equation (5), the material of the equivalent plate are in the plastic deformation stage.

$$\sigma = \frac{Et}{2\rho} \ge \sigma_s \quad (5)$$

The maximum stress produced by the outermost material is shown in the following equation:

$$\sigma_{max} = \sigma_s + K\left(\frac{t}{2\rho} - \frac{\sigma_s}{E}\right)^n \quad (6)$$

According to the equilibrium condition of external force and internal force, the bending moment of the cross section is obtained from the following integral calculation:

$$M = 2b\int_0^{t/2} y\sigma dy \quad (7)$$

With Equations (1)–(3), and (7),

$$M = \frac{2bEt_s{}^3}{3\rho} + \sigma_s b\left[\left(\frac{t}{2}\right)^2 - t_s{}^2\right] + 2Kb\int_{t_s}^{t/2} y\left(\frac{y}{\rho} - \frac{\sigma_s}{E}\right)^n dy \quad (8)$$

where b is the width of the cross section.

In order to simplify the integral calculation, the plastic strain is replaced by total strain approximately, $\varepsilon_p = \varepsilon = y/\rho$.

Hence, Equation (8) can be written as follows

$$M = \frac{2bEt_s{}^3}{3\rho} + \sigma_s b\left[\left(\frac{t}{2}\right)^2 - t_s{}^2\right] + \frac{2Kb}{(n+2)\rho^n}\left[\left(\frac{t}{2}\right)^{n+2} - t_s{}^{n+2}\right] \quad (9)$$

The elastic resilience value of the elastic-plastic bending is the change of elastic curvature produced by bending moment, as shown in Equation (10)

$$\frac{1}{\rho} - \frac{1}{\rho_{ae}} = \frac{M}{EI} \tag{10}$$

where I is the moment of inertia of the cross section, $I = bt^3/12$.

The bending radius of the SPM after springback can be obtained with Equations (9) and (10),

$$\rho_{ae} = \frac{\rho E b t^3}{E b t^3 - 12\left(\frac{2bEt_s^3}{3\rho} + \sigma_s b\left[\left(\frac{t}{2}\right)^2 - t_s^2\right] + \frac{2Kb}{(n+2)\rho^n}\left[\left(\frac{t}{2}\right)^{n+2} - t_s^{n+2}\right]\right)\rho} \tag{11}$$

As can be seen from Equation (11), b is included both numerator and denominator, hence the width of the cross section has no influence on the forming radius of the plate after unloading. Besides, in order to analyse under the same bending condition and process parameters, the ORM and SPM should keep the same thickness. Namely, width b and thickness t of the SPM are not as the equivalent parameters. In this work, σ_s, K, n are determined as the equivalent parameters of the SPM.

3.2.2. Bending Analysis of ORM

Integral panels are usually stiffened in both longitude and circumference. During the bending process, the deformation and stress of the longitudinal stiffened, which is parallel to the bending direction, are very small [30]. Therefore, the effect of the longitudinal reinforcement is ignored so that the analysis can be simplified. The distribution of the ribs and the simplified cross section of the ORM are shown in Figure 6.

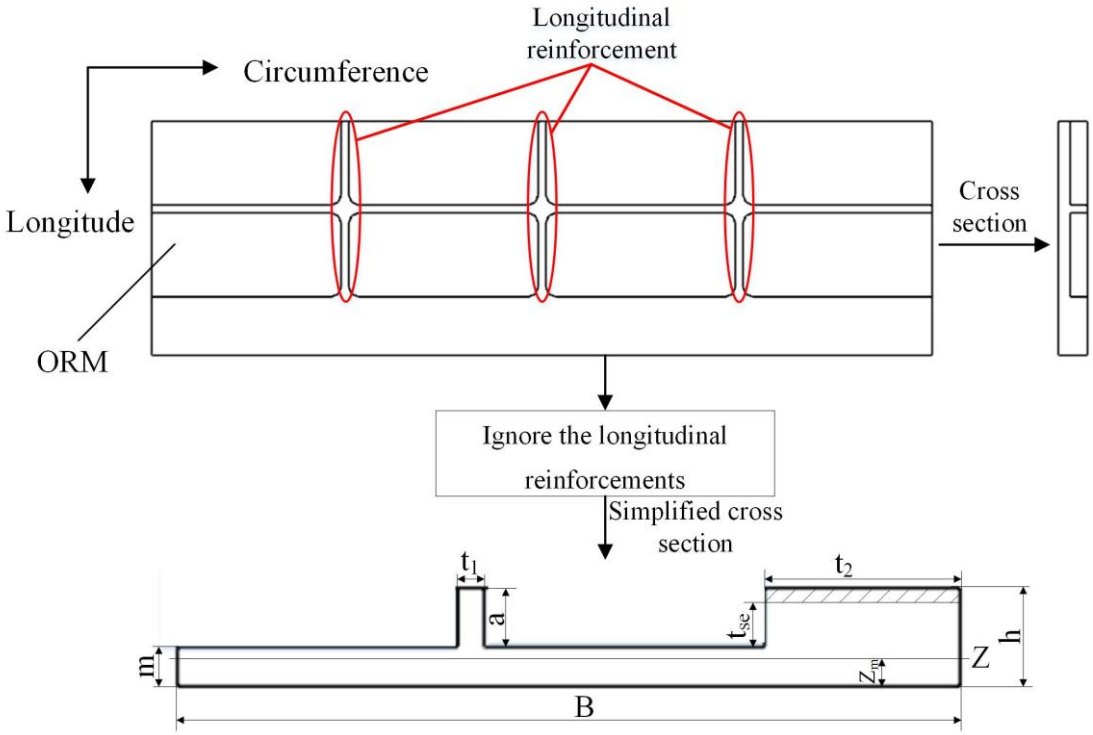

Figure 6. Simplified cross section of the ORM.

The centroid of the cross section is

$$Z_m = \frac{1/2Bm^2 + 1/2at_1^2 + amt_1 + 1/2t_2\left(h^2 - m^2\right)}{Bm + at_1 + t_2(h - m)} \tag{12}$$

From Equation (10), the same displacement deformation after springback of the SPM and ORM are obtained if Equation (13) is valid.

$$\frac{1}{\rho} - \frac{M}{EI} = \frac{1}{\rho_o} - \frac{M_o}{EI_o} \tag{13}$$

where I_o, M_o are the moment of inertia of the cross section and the bending moment after bending respectively. ρ_o is the bending radius of the neutral layer of ORM.

As shown in Figure 6, the origin of coordinate is on the axis of the centroid, the inertia moment of the ORM is obtained through integration.

$$\begin{aligned} I_o &= \int_{-Z_m}^{0} y^2 B dy + \int_{0}^{m-Z_m} y^2 B dy + \int_{m}^{h} y^2 t_1 dy + \int_{m}^{h} y^2 t_2 dy \\ &= \frac{BZ_m{}^3 + B(m-Z_m)^3 + t_1\left(h^3 - m^3\right) + t_2\left(h^3 - m^3\right)}{3} \end{aligned} \tag{14}$$

The bending moment of the neutral layer in the transverse section located under the punch of the ORM is,

$$M_o = \int_{-Z_m}^{0} y\sigma B dy + \int_{0}^{m} y\sigma B dy + \int_{m}^{h} y\sigma t_1 dy + \int_{m}^{m+t_{se}} y\sigma t_2 dy + \int_{m+t_{se}}^{h} y\sigma t_2 dy \tag{15}$$

where t_{se} is the distance between the plastic deformation zone and the elastic deformation zone to the bottom of the rib,

$$t_{se} = \frac{\rho_D \sigma_{so}}{E} + Z_m - m \tag{16}$$

Substituting Equation (1) into Equation (15), the bending moment can be described by

$$\begin{aligned} M_o = {} & BE\int_{-Z_m}^{0} \varepsilon y dy + BE\int_{0}^{m} \varepsilon y dy + t_1 E\int_{m}^{h} \varepsilon y dy + t_2 E\int_{m}^{m+t_{se}} \varepsilon y dy + t_2\int_{m+t_{se}}^{h} y\left[\sigma_s + K|\varepsilon_p|^{n_o}\right] dy \\ = {} & \frac{BEZ_m{}^3}{3\rho_D} + \frac{BE}{3\rho_D} m^3 + \frac{t_1 E}{3\rho_D}\left[h^3 - m^3\right] + \frac{t_2 E}{3\rho_D}\left[(m+t_{se})^3 - m^3\right] + \frac{t_2\sigma_{so}}{2}\left[h^2 - (m+t_{se})^2\right] + \\ & \frac{t_2 K}{(n_o+2)\rho_D{}^{n_o}}\left[h^{n_o+2} - (m+t_{se})^{n_o+2}\right] \end{aligned} \tag{17}$$

Substituting Equation (17) into Equation (10), the forming radius of the ORM after unloading is given by

$$\rho_{oae} = \frac{EI_o\rho_o}{EI_o - \rho_o M_o} \tag{18}$$

When the outer stress of the material reaches Equation (19), the material of the ORM are in the plastic deformation phase.

$$\sigma_o = \frac{E(h - Z_m)}{\rho_o} \geq \sigma_{so} \tag{19}$$

The maximum stress produced by the outermost material is

$$\sigma_{omax} = \sigma_{so} + K_o\left(\frac{h - Z_m}{\rho_o} - \frac{\sigma_{so}}{E}\right)^{n_o} \tag{20}$$

3.2.3. Equivalent Parameters

According to equivalent requirements, the following three conditions are required to meet: (i) the material begin to be yielded simultaneously; and (ii) the ultimate stress of the ORM is the same as that of the SPM at the same punch displacement; (iii) the forming radii of neutral surfaces of the ORM and the SPM are identical after springback.

The forming radius of neutral layer of the SPM and the ORM have the following relation:

$$\rho = \rho_o + Z_m - \frac{t}{2} \tag{21}$$

The thickness of the SPM and the ORM is the same, namely $h = t$. According to the first condition of the equivalent requirements, (i), and with the Equations (5), (19) and (21), Equation (22) is given by

$$\frac{Et}{2\sigma_s} = \frac{E(h - Z_m)}{\sigma_{so}} + Z_m - \frac{t}{2} \tag{22}$$

According to the second condition, (ii), Equation (23) can be derived as follows by Equations (6), (20) and (21).

$$\sigma_s + K\left(\frac{t}{2\rho} - \frac{\sigma_s}{E}\right)^n = \sigma_{so} + K_o\left(\frac{h - Z_m}{\rho_o} - \frac{\sigma_{so}}{E}\right)^{n_o} \tag{23}$$

According to the third condition, (iii), and with the Equations (11), (13), (18) and (21), Equation (24) is derived as

$$\frac{\rho E b t^3}{E b t^3 - 12 M \rho} = \frac{E I_o (2\rho + h - 2Z_m)}{2 E I_o - M_o (2\rho + h - 2Z_m)} \tag{24}$$

Based on the above derivation, Equation (22) is solved for the yield stress of the SPM, σ_s. Hardening coefficient (K) and hardening exponent (n) can be obtained by combining Equations (23) and (24). In the case of the ORM with other complex structure, the equivalent calculation method is similar. The full procedure of the method is shown in Figure 7.

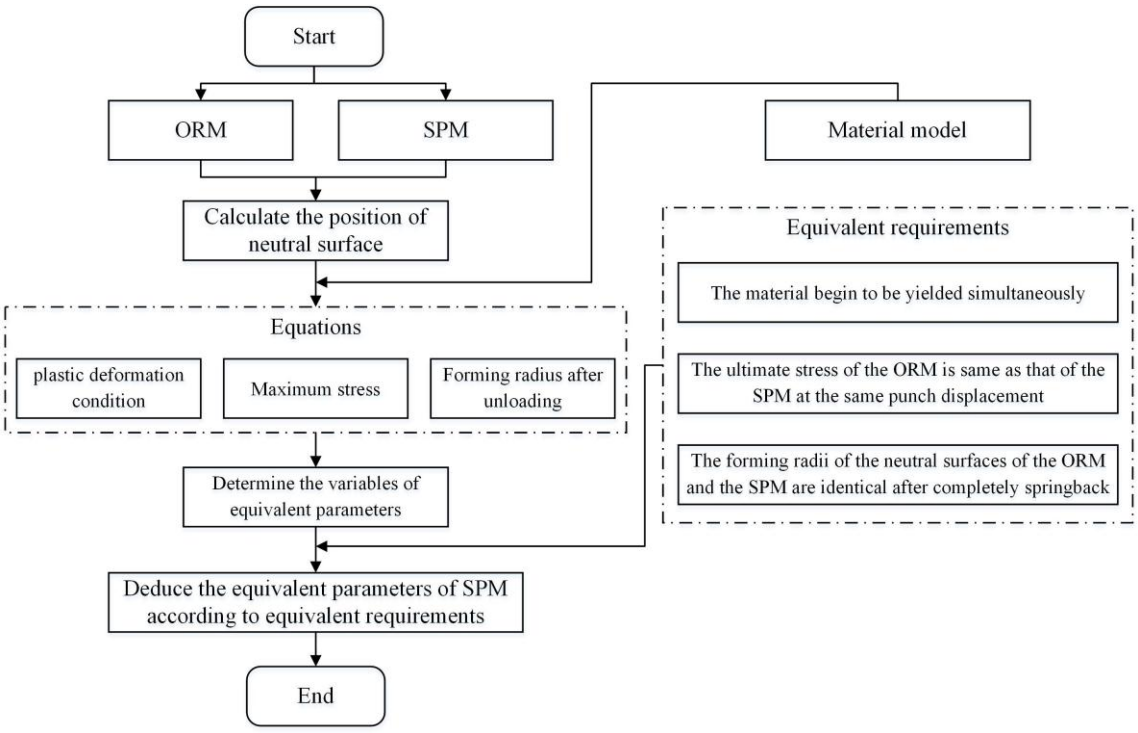

Figure 7. The full procedure of the equivalent calculation method.

4. Simulation and Experimental Verification

4.1. FE Simulation Model

In order to verify the validity of the proposed method, FE simulation is carried out to simulate the formation of the ORM and the SPM. The material is 7050-T7451 aluminum alloy, and the properties are obtained with uniaxial tensile test on the CSS-44100 Electric Universal Testing Machine at a rate of 1.5 mm/min until fracture occurs, as shown in Figure 8. The dimensions of tensile coupons are designed according to the national standard GB/T228-2002 *Metal Material Room Temperature Tensile Test Method*, as shown in Figure 8a. The tensile process is shown in Figure 8b and the tensile stress-strain

curves are plotted in Figure 8c (average). The forming parameters and material properties of the material are summarized in Table 1, which are used to create the FE models.

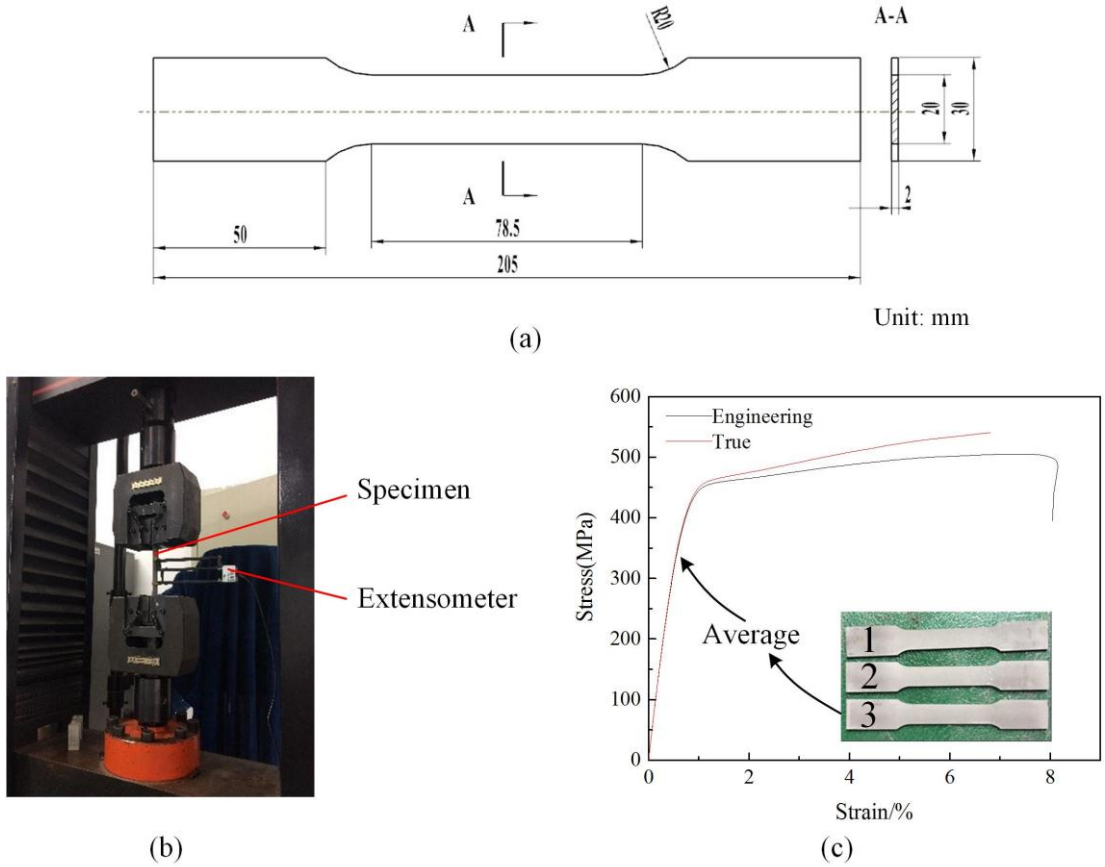

Figure 8. Uniaxial tensile test (**a**) geometric parameters of specimen (**b**) tensile process (**c**) Engineering and true stress-strain curve.

Table 1. Forming parameters and material properties.

Items		Parameters	Values	Items		Parameters	Values
FE model parameters	ORM	L	200 mm	Material properties	ORM	E	66,000 MPa
		B	60 mm			ν	0. 33
		h	7.5 mm			σ_{so}	442 MPa
		t_1	2 mm			K_o	778.8
		t_2	15 mm			n_o	0.73
		a	4.5 mm		SPM	E	66,000 MPa
	SPM	l	200 mm			ν	0.33
		b	15 mm			σ_s	339.87 MPa
		t	7.5 mm			K	363.635
	Tools	d_1,d_2	15 mm			n	0.148

An FE simulation of the forming process is performed via the Abaqus 6.14 platform. The explicit algorithm of Abaqus/explicit module fitted for dynamic and non-linear analysis is used to simulate the bending process and the implicit algorithm of Abaqus/standard module adapted to static and steady analysis is used for springback simulation [31]. The punch and support bodies are considered as rigid bodies in comparison with the deformable plate [32,33]. The FE model consists of four main components: three rigid tools and one flexible plate, which are illustrated in Figure 9. 3D brick elements (C3D8R) are used to mesh the flexible models, and rigid discrete elements (R3D4) are selected

to describe the discrete rigid tools. The exponential strengthening material model is used to represent the elastoplastic behavior obtained from uniaxial tensile tests. The contact type between the workpiece and the die is automatic surface–surface [34], and the workpiece is driven and deformed to the bending plate through these contact surfaces.

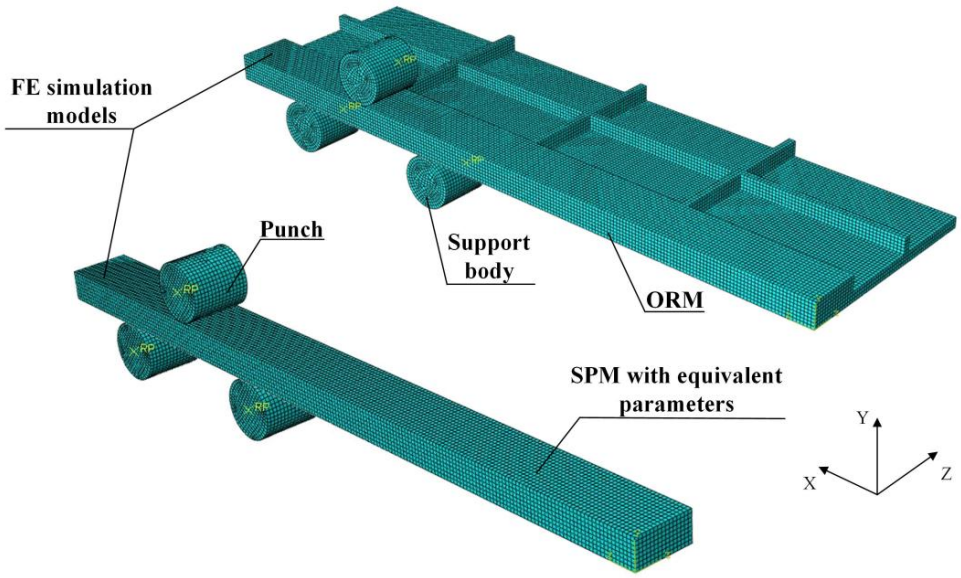

Figure 9. FE simulation models of SPM and ORM.

4.2. Bending Experiment

The CSS-44100 Electric Universal Testing Machine is used to validate the FE simulation model. The radius of both the punch and the support bodies are 15 mm, and the distance between the support bodies is 50 mm. The displacement of both the left and right bending points are 3 mm and the intermediate bending point is 3.5 mm. The loading positions (1), (2) and (3) are indicated in Figure 10. The measurement points are used to obtain the contour data of the bent specimen after unloading using portable 3D Photograph Meter.

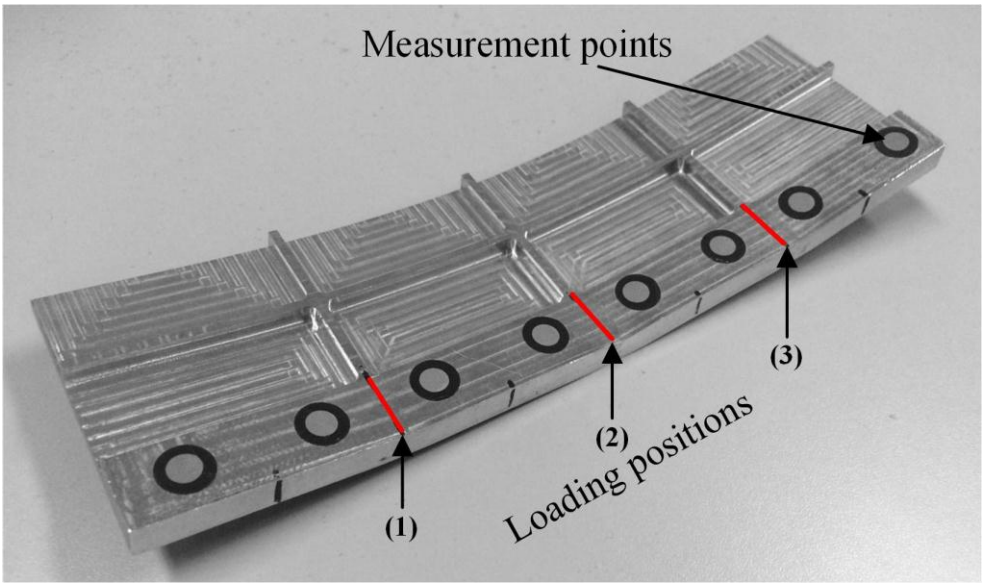

Figure 10. Bending experiment of ORM.

5. Results and Discussion

In this section, the experimental and simulation results are compared and analyzed. The final shapes and stresses distribution of the ORM and SPM are obtained and discussed respectively. The efficiency of FE simulation calculated with SPM is compared with ORM analysis.

5.1. Distribution of Stress and Strain

The successive forming process and the stress distribution of the SPM and the ORM can be seen in Figure 11, depicting the equivalent Mises stress in different loading positions of the formation process. It is seen that the Mises stress increases when the punch displacement increases from 3 mm to 3.5 mm, and as expected, the maximum Mises stresses are concentrated below the indenter and the bottom surface of the bent specimens. This stress distribution after punch displacement is consistent with the previous work by Anokye-Siribor [35], which means that the metal farther away from the neutral axis has been stressed beyond the yield strength, and has been plastically or permanently deformed. The maximum relative error of Mises stress between the SPM and ORM is 7.78%. Furthermore, it can be observed that the maximum Mises stress of the SPM is greater than that of the ORM; the difference may be due to the calculation error of the equivalent parameters. However, it is beneficial to ensure the forming quality of the ORM.

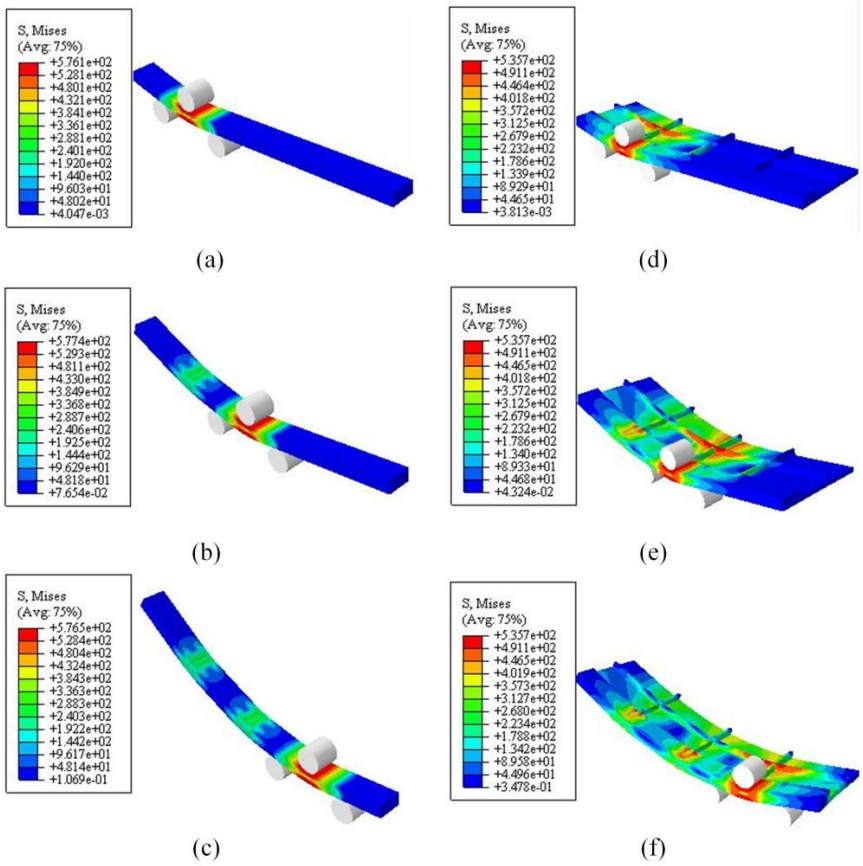

Figure 11. Mises stress distribution of SPM (**a**–**c**) and ORM (**d**–**f**) at three loading positions.

In the longitudinal direction, the residual stresses distribution of the SPM and the ORM after bending and springback at the end of the simulations are shown in Figure 12. The distribution is consistent with the research results of literature [36,37]. Namely, springback relaxes a large amount of stress and causes the tensile and compressive stresses to have their largest values near the neutral layer.

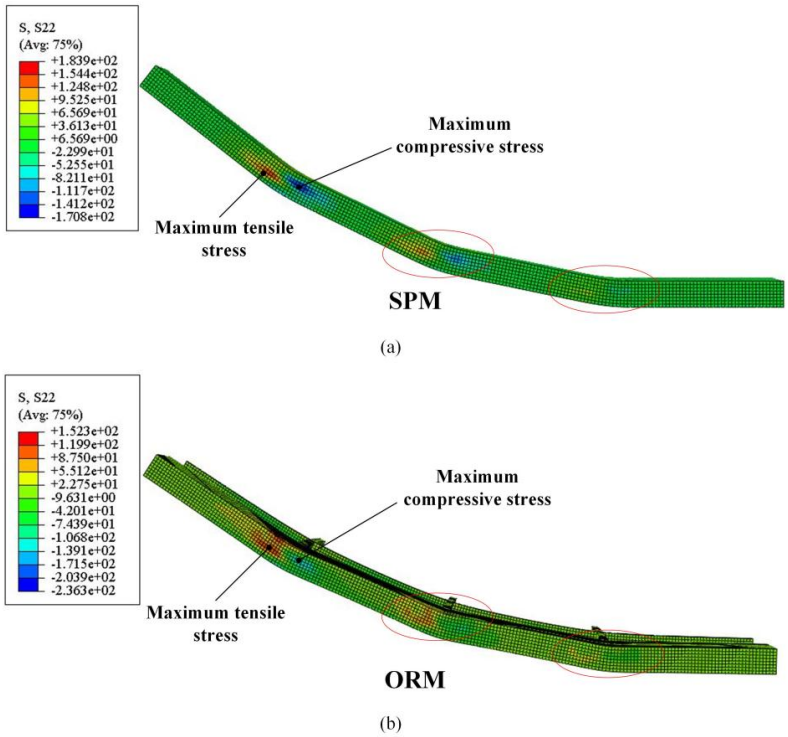

Figure 12. Longitudinal residual stress distribution of SPM (**a**) and ORM (**b**).

The equivalent plastic strains distribution in the longitudinal direction and through the thickness direction below the punch of the formed specimens after releasing the loading are shown in Figure 13. The simulation results reveal that the maximum strains are mainly concentrated on specimen surfaces due to structural bending, and the strains away from the punch remain low.

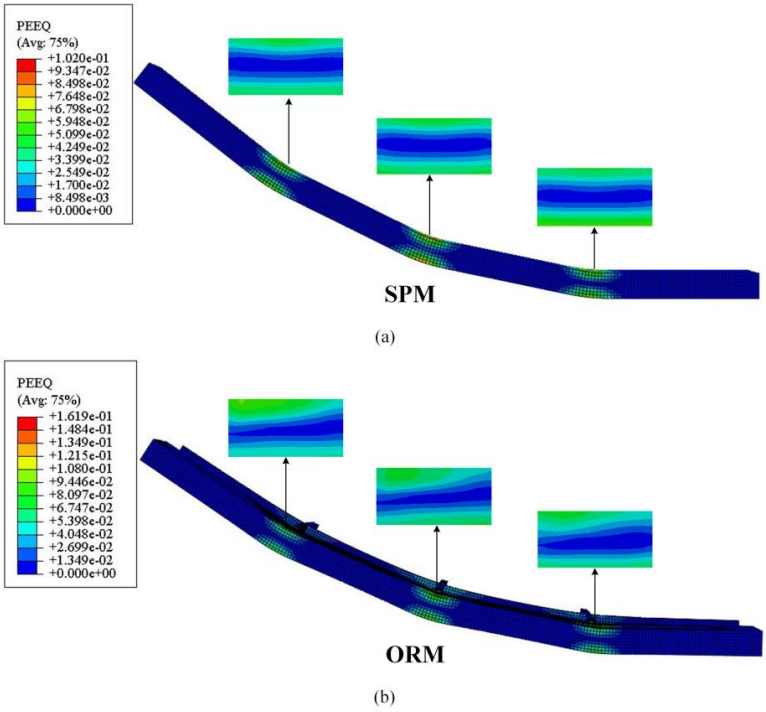

Figure 13. Equivalent plastic strain distribution of SPM (**a**) and ORM (**b**).

5.2. Contours of the Forming Workpieces

To verify the geometry of the final shapes of the forming workpieces after springback, the contour figure data of the ORM and the SPM are obtained from the FE simulation models when the forming processes are completed, as illustrated in Figures 12 and 13. A good agreement between the SPM and the ORM can be observed in Figure 14, and the calculated error is less than 13.17%. Therefore, the SPM can simulate the bending forming of the ORM quite well. Compared with the experimental results, the deformation error of the ORM is slightly smaller than that of the SPM. The error between the FE simulations and the experimental results may result from the assumptions for theoretical analysis and FE simulation of bending process, and the error of the contour data of the bent specimen result from both the measurement method and fitting method. Moreover, the accuracy of indenter displacement also affects the final shapes of the forming workpieces in the bending experiment.

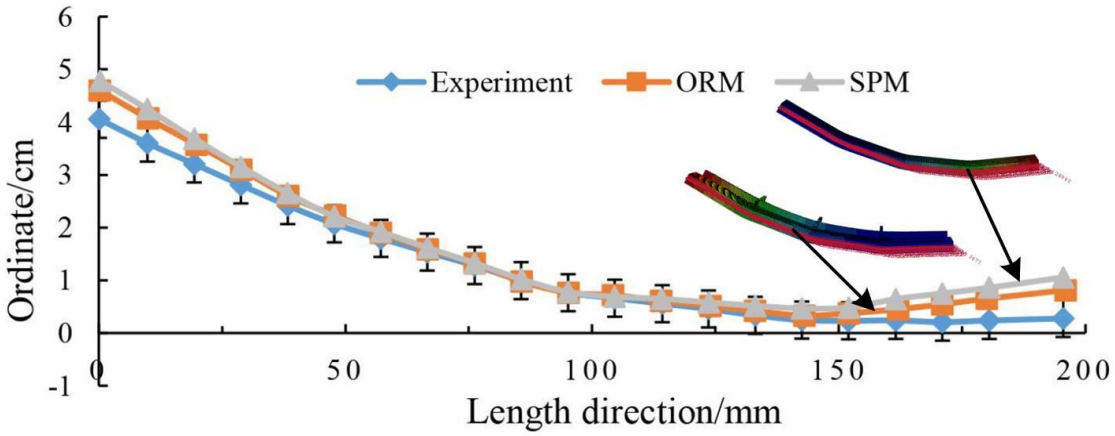

Figure 14. Comparison of contours.

5.3. Comparing the Reaction Force between FE Simulation and Experiment

Figure 15 shows the comparison of the reaction force between FE simulation and experiment in the cases of punch displacement 3 mm and 3.5 mm. The FE simulation results of ORM show a good agreement with the experimental results. It is observed that the reaction force increases as the punch displacement increases. However, the error of the simulation results of SPM as compared with the experimental results is larger. The difference mainly results from factors such as ignoring the position change of the neutral surface, the error of material model, and the influence of the shear stress when calculating the equivalent parameters. It is also observed that the reaction force is zero with increasing punch displacement at the beginning of loading and the punch displacements exceed 3 mm and 3.5 mm at the end of loading in the FE simulation results, because the punch and support bodies are not fully contacted with the specimen in the assembly model and there is a 0.1 mm gap between them to ensure the convergence of FE calculation.

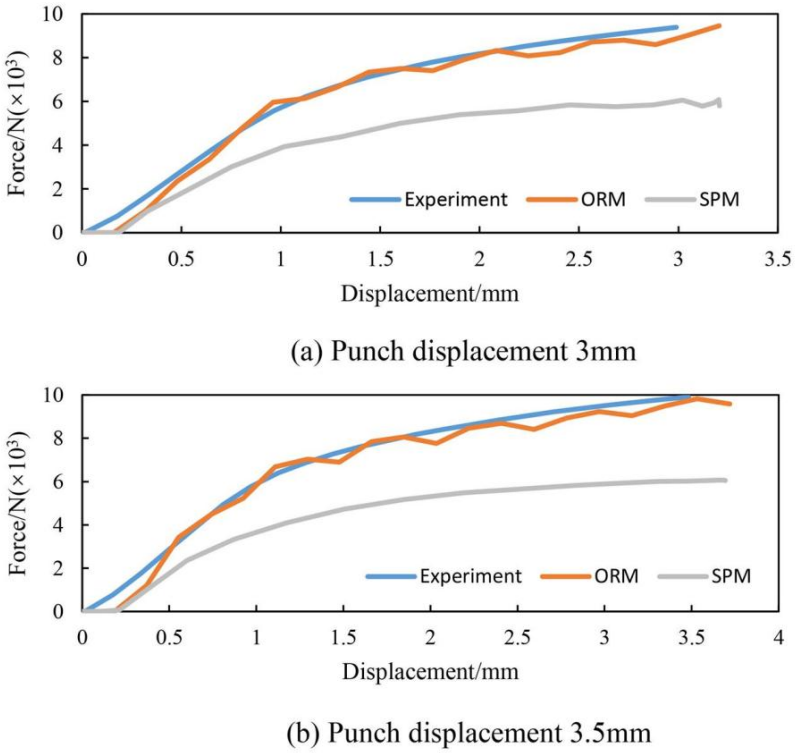

Figure 15. Comparison of the rection force between FE simulation and experiment.

5.4. Efficiency Analysis

In terms of the efficiency of the FE simulation, the calculation time of the ORM and the SPM are compared in Figure 16. The efficiency has been improved by more than 48%. In terms of the structure, the SPM is consistent with the area of bending load applying of the ORM. Therefore, the SPM can replace the ORM in the optimization of bending process to lower the amount of iterative calculation. The efficiency of modeling and calculation can greatly improve, and the computing non-convergence is avoided.

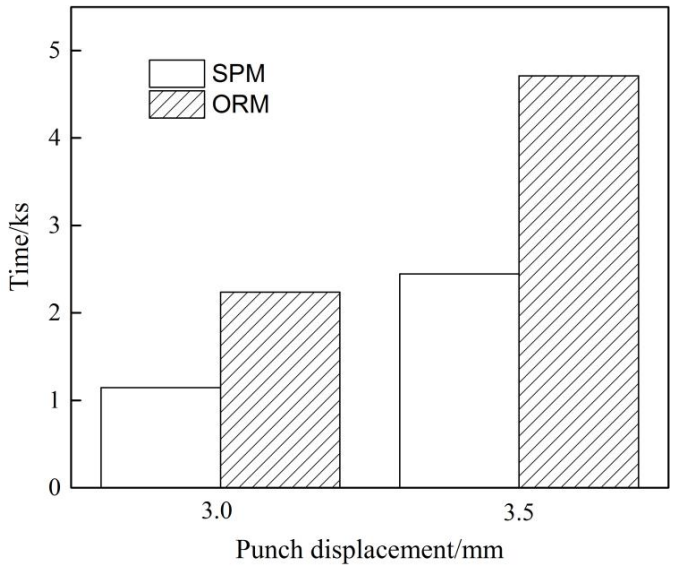

Figure 16. Calculation time of ORM and SPM.

6. Conclusions

An equivalent calculation method for press-braking bending analysis of integral panels is proposed to solve the problem that long-time calculation and extensive computational resources are required for simulating the bending forming process with an ORM. The main conclusions are as follows:

(1) With the detailed analysis of the bending forming and springback of the SPM and ORM, the equivalent parameters for the SPM including the yield stress σ_s, hardening coefficient K and hardening exponent n are determined and obtained according to the equivalent requirements.
(2) The FE simulation is carried out to simulate the bending forming of the ORM and the SPM. The simulation results indicate that the maximum relative error of Mises stress between the SPM and ORM is 7.78%, and the calculated error of contours between ORM and SPM is less than 13.17%.
(3) The fact that the SPM has a similar stress distribution and contour curve comparing with the ORM under the same forming parameters, suggests that the SPM can replace the ORM in the FE simulation to avoid a large number of mesh generation and in the optimization of bending process to lower the amount of iterative calculation.
(4) Compared with ORM, the calculating efficiency of the FE simulation with SPM is improved significantly (by more than 48%), while ensuring simulation accuracy.

To improve the simulation accuracy, the anisotropy of the material should be taken into account in the FE simulation of the forming process. The effect of machining-induced residual stress on the accuracy of the simulation should be further studied.

Author Contributions: M.Z. performed the experiments, simulation and wrote the paper under the guidance of the corresponding author X.T.; W.L. and X.S. assisted in analyzing the data and discussing the results.

Funding: This research received no external funding.

Conflicts of Interest: The authors declare no conflict of interest.

References

1. Zeng, Y.S.; Huang, X. Forming technologies of large integral panel. *Acta Aeronaut. Astronaut. Sin.* **2008**, *29*, 721–727.
2. Luo, H.; Li, W.D.; Li, C.; Wan, M. Investigation of creep-age forming of aluminum lithium alloy stiffened panel with complex structures and variable curvature. *Int. J. Adv. Manuf. Technol.* **2017**, *91*, 3265–3271. [CrossRef]
3. Liu, C.G.; Li, J.; Dong, Y.N.; Zhang, X.G.; Yue, T. Fracture prediction in the forming of aircraft Al stiffeners using multi-point dies. *Int. J. Adv. Manuf. Technol.* **2017**, *90*, 3109–3118. [CrossRef]
4. Thipprakmas, S. Finite element analysis of punch height effect on V-bending angle. *Mater. Des.* **2010**, *31*, 1593–1598. [CrossRef]
5. Kuroda, K.; Kawakami, T.; Okui, T.; Akiyama, M.; Kiuchi, M. Influential factor to dimensional precision of cold-drawn tubes. *Proc. Inst. Mech. Eng. B J. Eng.* **2015**, *229*, 100–109. [CrossRef]
6. Panthi, S.K.; Ramakrishnan, N.; Ahmed, M.; Singh, S.S.; Goel, M.D. Finite Element Analysis of sheet metal bending process to predict the springback. *Mater. Des.* **2010**, *31*, 657–662. [CrossRef]
7. Li, W.D.; Wan, M. Press bending equivalent simulation model of integrally reinforced panel. *J. Beijing. Univ. Aeronaut. Astronaut.* **2014**, *40*, 1537–1542.
8. Chongthairungruang, B.; Uthaisangsuk, V.; Suranuntchai, S.; Jirathearanat, S. Springback prediction in sheet metal forming of high strength steels. *Mater. Des.* **2013**, *50*, 253–266. [CrossRef]
9. Cao, T.S. Models for ductile damage and fracture prediction in cold bulk metal forming processes: A review. *Int. J. Mater. Form.* **2015**, *10*, 1–33. [CrossRef]
10. Wen, H.B.; Li, W.D.; Wan, M. Prediction and analysis of stiffener buckling in press bend forming of integral panels. *J. Plast. Eng.* **2013**, *20*, 56–60.

11. Benedetti, M.; Fontanari, V.; Monelli, B.; Tassan, M. Single-point incremental forming of sheet metals: Experimental study and numerical simulation. *Proc. Inst. Mech. Eng. B J. Eng.* **2017**, *231*, 301–312. [CrossRef]
12. Fu, Z.M.; Tian, X.L.; Chen, W.; Hu, B.K.; Yao, X.Y. Analytical modeling and numerical simulation for three-roll bending forming of sheet metal. *Int. J. Adv. Manuf. Technol.* **2013**, *69*, 1639–1647. [CrossRef]
13. Xia, J.; Lu, S.H. 3D FEM Simulation and Experimental Research of Springback in Bending Process of Aluminum Alloy Sheet. *Key Eng. Mater.* **2010**, *431–432*, 487–490.
14. Muhammad, A.A.; Ala, Q. Numerical simulation of sheet metal forming: A review. *Int. J. Adv. Manuf. Technol.* **2017**, *89*, 1235–1250.
15. Ghaei, A.; Green, D.E.; Aryanpour, A. Springback simulation of advanced high strength steels considering nonlinear elastic unloading—Reloading behavior. *Mater. Des.* **2015**, *88*, 461–470. [CrossRef]
16. Tran, Q.H.; Champliaud, H.; Feng, Z.K.; Dao, T.M. Analysis of the asymmetrical roll bending process through dynamic FE simulations and experimental study. *Int. J. Adv. Manuf. Technol.* **2014**, *75*, 1233–1244. [CrossRef]
17. Zhao, G.Y.; Liu, Y.L.; Yang, H.; Lu, C.H.; Gu, R.J. Three-dimensional finite-elements modeling and simulation of rotary-draw bending process for thin-walled rectangular tube. *Mater. Sci. Eng. A Struct.* **2009**, *499*, 257–261. [CrossRef]
18. Fu, Z.M.; Chen, W.; Tian, X.L.; Hu, B.K. Modeling and simulation for multiple-step incremental air-bending forming of sheet metal. *Int. J. Adv. Manuf. Technol.* **2014**, *72*, 561–570. [CrossRef]
19. Fu, Z.M.; Mo, J.H. Multiple-Step Incremental Air-Bending Forming of High-Strength Sheet Metal Based on Simulation Analysis. *Mater. Manuf. Process.* **2010**, *25*, 808–816. [CrossRef]
20. Henrard, C.; Bouffioux, C.; Eyckens, P.; Sol, H.; Duflou, J.R.; Houtte, P.V.; Bael, A.V.; Duchêne, L.; Habraken, A.M. Forming forces in single point incremental forming: Prediction by finite element simulations, validation and sensitivity. *Comput. Mech.* **2011**, *47*, 573–590. [CrossRef]
21. Bui, Q.V.; Ponthot, J.P. Numerical simulation of cold roll-forming processes. *J. Mater. Process. Technol.* **2008**, *202*, 275–282. [CrossRef]
22. Yan, Y.; Wan, M.; Wang, H.B. FEM equivalent model for press bend forming of aircraft integral panel. *Trans. Nonferrous Met. Soc.* **2009**, *19*, 414–421. [CrossRef]
23. Xia, L.J.; Jin, X.D.; Wang, Y.B. The equivalent analysis of honeycomb sandwich plates for satellite structure. *J. Shanghai Jiaotong Univ.* **2003**, *37*, 999–1001.
24. Zhang, T.L.; Ding, Y.L.; Jin, H.B. Comparative analysis of equivalent models for honeycomb sandwich plates. *Chin. J. Appl. Mech.* **2011**, *28*, 275–282.
25. Liang, S.; Chen, H.L.; Chen, T.N.; Liang, T.X. Analytical study of the equivalent elastic parameters for a honeycomb core. *J. Aeronaut. Mater.* **2004**, *24*, 26–31.
26. Chen, X.A.; Zhang, Y.Y.; Hu, G.T.; Zeng, Q.N.; Liu, H.; Fang, J.Z. Analysis of Equivalent Parameters for Honeycomb Sandwich Mirror. *Adv. Mater. Res.* **2014**, *842*, 397–400. [CrossRef]
27. Yang, J.S.; Li, D.L.; Ma, L.; Zhang, S.Q.; Schröder, K.U.; Schmidt, R. Numerical static and dynamic analyses of improved equivalent models for corrugated sandwich structures. *Mech. Adv. Mater. Struct.* **2018**, 1–12. [CrossRef]
28. Trzepiecinski, T.; Lemu, H.G. Effect of Computational Parameters on Springback Prediction by Numerical Simulation. *Metals(Basel)* **2017**, *7*, 380. [CrossRef]
29. Wagoner, R.H.; LI, M. Simulation of springback: Through-thickness integration. *Int. J. Plast.* **2007**, *23*, 345–360. [CrossRef]
30. Lai, S.B.; Yu, D.Y.; Chen, T.X. Plastic Equivalent Model for Integrally Stiffened Panel in Bending Forming. *J. Astronaut.* **2012**, *33*, 809–815.
31. Abebe, M.; Yoon, J.S.; Kang, B.S. Radial Basis Functional Model of Multi-Point Dieless Forming Process for Springback Reduction and Compensation. *Metals (Basel)* **2017**, *7*, 528. [CrossRef]
32. Feng, Z.K.; Champliaud, H. Three-stage process for improving roll bending quality. *Simul. Model. Pract. Theory* **2011**, *19*, 887–898. [CrossRef]
33. Feng, Z.K.; Champliaud, H. Modeling and simulation of asymmetrical three-roll bending process. *Simul. Model. Pract. Theory* **2011**, *19*, 1913–1917. [CrossRef]
34. Tan, J.Q.; Zhan, M.; Gao, P.F.; Li, H.W. Electromagnetic Forming Rules of a Stiffened Panel with Grid Ribs. *Metals (Basel).* **2017**, *7*, 559. [CrossRef]
35. Anokye-Siribor, K.; Singh, U.P. A new analytical model for pressbrake forming using in-process identification of material characteristics. *J. Mater. Process. Technol.* **2000**, *99*, 103–112. [CrossRef]

36. Liu, B.; Villavicencio, R.; Soares, C.G. Experimental and numerical analysis of residual stresses and strains induced during cold bending of thick steel plates. *Mar. Struct.* **2018**, *57*, 121–132. [CrossRef]
37. Jiang, Z.Q.; Yang, H.; Zhan, M.; Yue, Y.B.; Liu, J.; Xu, X.D.; Li, G.J. Establishment of a 3D FE model for the bending of a titanium alloy tube. *Int. J. Mech. Sci.* **2010**, *52*, 1115–1124. [CrossRef]